Nanoscale

PAPER

Cite this: *Nanoscale*, 2014, **6**, 15236

Spatial temperature mapping within polymer nanocomposites undergoing ultrafast photothermal heating *via* gold nanorods†

Somsubhra Maity,[a] Wei-Chen Wu,[b] Chao Xu,[a] Joseph B. Tracy,[b] Kenan Gundogdu,[a] Jason R. Bochinski*[a] and Laura I. Clarke*[a]

Received 6th September 2014,
Accepted 26th October 2014

DOI: 10.1039/c4nr05179c

www.rsc.org/nanoscale

Heat emanates from gold nanorods (GNRs) under ultrafast optical excitation of the localized surface plasmon resonance. The steady state nanoscale temperature distribution formed within a polymer matrix embedded with GNRs undergoing pulsed femtosecond photothermal heating is determined experimentally using two independent ensemble optical techniques. Physical rotation of the nanorods reveals the average local temperature of the polymer melt in the immediate spatial volume surrounding each rod while fluorescence of homogeneously-distributed perylene molecules monitors temperature over sample regions at larger distances from the GNRs. Polarization-sensitive fluorescence measurements of the perylene probes provide an estimate of the average size of the quasi-molten region surrounding each nanorod (that is, the boundary between softened polymer and solid material as the temperature decreases radially away from each particle) and distinguishes the steady state temperature in the solid and melt regions. Combining these separate methods enables nanoscale spatial mapping of the average steady state temperature distribution caused by ultrafast excitation of the GNRs. These observations definitively demonstrate the presence of a steady-state temperature gradient and indicate that localized heating *via* the photothermal effect within materials enables nanoscale thermal manipulations without significantly altering the bulk sample temperature in these systems. These quantitative results are further verified by re-orienting nanorods within a solid polymer nanofiber without inducing any morphological changes to the highly temperature-sensitive nanofiber surface. Temperature differences of 70–90 °C were observed over a distances of ~100 nm.

1. Introduction

Metal nanoparticles incorporated into media act as versatile nanoscale heaters, converting light into heat.[1,2] The large absorption cross-section (typically, larger than the physical geometric cross-section of the object[3] and orders of magnitude greater than organic fluorophores[4]) for illumination resonant with the nanoparticle's localized surface plasmon (SPR) and the rapid, efficient light-to-heat energy conversion of the photothermal process make metal nanoparticles ideal tools for wide-ranging scientific applications. Such diverse applied and fundamental research uses include nanoscale control of heat generation,[5–8] heat-induced actuation,[9–11] thermally-assisted material growth[12] and lithographic patterning,[6,13] controllable phase transformations,[14,15] and high density optical storage,[16–19] as well as biomedical uses[20,21] such as cancer therapy[4,22,23] and drug[24,25] and chemical delivery.[26,27] The SPR frequency for spherically-shaped particles can be altered through choice of particle composition and size. However facile SPR tuning is most readily achieved by utilizing a spatially anisotropic shape (*e.g.*, nanorods).[28] The anisotropic shape of nanorods produces two distinct localized surface plasmon modes corresponding to the transverse (TSPR) and longitudinal (LSPR) axes of the nanoparticle.[29] The spectral location of the LSPR depends on the particle length-to-width aspect ratio (AR); with higher AR the LSPR shifts toward longer wavelengths while the TSPR is essentially unaffected. For example, the LSPR wavelength for a GNR can be readily adjusted across the visible and near-infrared (NIR) spectrum through selection of appropriate AR,[29] allowing utilization of optimal sample penetrating regions of the spectrum for certain applications (*e.g.*, the first NIR window[30] between ~650–950 nm for biological tissues), whereas the TSPR stays relatively unchanged around 520 nm.

[a]*Department of Physics, North Carolina State University, Raleigh, NC, 27695-8202 USA. E-mail: laura_clarke@ncsu.edu, jason_bochinski@ncsu.edu*
[b]*Department of Materials Science and Engineering, North Carolina State University, Raleigh, NC, 27695 USA*
†Electronic supplementary information (ESI) available. See DOI: 10.1039/C4NR05179C

This journal is © The Royal Society of Chemistry 2014

Pulsed laser irradiation of metal nanoparticles is known to produce dramatic temperature increases and facilitate acoustic wave generation,[31] nanosurgery,[32–36] bubble formation[37–39] and nanoparticle reshaping.[40] A robust and direct experimental measurement of the resultant temperature distribution when embedding nanorods in different media is useful to gain understanding of the important experimental parameters that determine the steady state temperature distribution when undergoing photothermal heating. While many theoretical treatments[5,41–51] and some experimental temperature measurements[7,43,52–54] have appeared, most work has investigated these nanoscale heaters when surrounded by fluid (*i.e.*, primarily water), with fewer reports discussing such effects within solid-phase material, highly-viscous fluid environments,[7] or potentially more complex material phase combinations.

In the present work, an experimental method is demonstrated for directly measuring the average steady state temperature resulting from ultrafast pulsed irradiation of nanorods in a polymer matrix within three distinct nanoscale spatial regions at different distances from the GNR. The polymer is doped with aligned GNRs and an ultrafast laser resonant with the LSPR generates photothermal heat from the dispersed nanoscale sources, causing localized melting of the polymer. The temperature of the polymer melt immediately surrounding each GNR is inferred from monitoring nanorod rotational dynamics within the viscous polymer melt by observing the transmission of a weak probe beam. This ensemble optical measurement begins with all nanoparticles aligned and observes thermal randomization or forced reorientation of the GNRs through the resultant change in sample transmission, connecting the response time with the melt temperature *via* a robust calibration. The temperature of the matrix in regions further from the surfaces of the GNRs is independently and simultaneously detected by polarized fluorescence measurements of dilute, perylene molecules homogeneously-distributed throughout the sample. Calibrated analysis of the emission signals reveals temperature information about the molten and solid sample regions by distinguishing between fixed molecules and those able to rotationally re-orient. This analysis also provides an estimate of the size of the molten region surrounding each nanorod. The observations unequivocally demonstrate that a steady state thermal gradient from the nanorod outward is continuously maintained within the polymer nanocomposite samples under ultrafast excitation.

To verify the independently measured temperature profile, experiments were conducted within temperature-sensitive polymeric nanofibers, where the maximum temperature history of the nanofiber surface can be readily shown by examining fiber morphology after thermal treatment. Explicit reorientation of GNRs in this environment was monitored optically and confirmed by electron microscopy, definitively establishing that the immediate local volume surrounding the nanorod was molten while simultaneously cooler temperatures were maintained over distances of less than 200 nm.

2. Results and discussion

2.1. Aligning GNRs within the nanocomposite

GNRs obtained using a seed-mediated synthesis[55] had average lengths of 68 ± 7 nm long, widths of 17 ± 3 nm, and an AR of 4.0 ± 0.82. The GNRs were coated with ~4 nm thick shells of silica (see ESI†), to which polyethylene glycol (PEG) was grafted, providing good solubility in methanol. Polyethylene oxide (PEO) nanocomposite films were produced by drop-casting a GNR–PEO–perylene solution to obtain a thin film with thickness of ~8 μm. Perylene is utilized to monitor sample internal temperature as discussed below. For the samples here, based on the GNR concentration used, the average center-to-center separation between nanorods is ~270 nm in the final nanocomposite sample. Film samples were dried under ambient conditions with a horizontally applied external DC electric field (20 kV cm^{-1}) which orients the GNRs parallel to the electric field direction through an induced dipole moment[56] and aligning torque,[57] as opposed to using mechanical methods.[58,59] This procedure creates a nanocomposite film with the ensemble gold nanorods aligned with high orientation fidelity along one specified direction (Fig. 1(b)). Additionally, samples comprised of composite nanofibers were also generated by needle electrospinning,[60,61] producing nanofibers ~250 ± 30 nm in diameter collected with random fiber orientation in layers as a nanofibrous mat. Due to both the electric field and polymer solution flow-induced shear present during the electrospinning process, GNRs embedded within polymer nanofibers are well aligned along the fiber axis (Fig. 1(c)).[62,63]

As discussed above, the anisotropic shape of GNRs produces two spectrally distinct localized surface plasmon

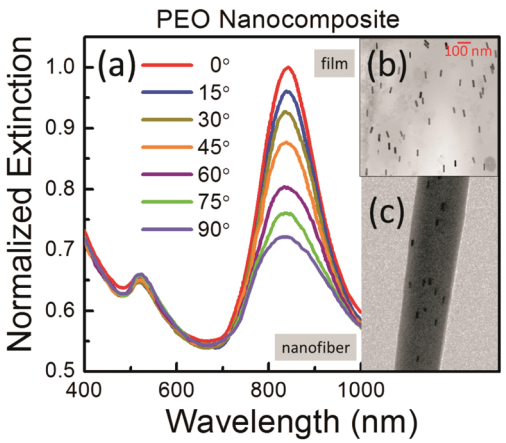

Fig. 1 (a) Linearly-polarized extinction spectrum of aligned GNR in PEO nanocomposite. The angle-dependent extinction validates the anisotropic nature of the sample where maximum extinction occurs for parallel polarization and GNR orientation and minimum extinction for the orthogonal configuration. TEM images of (b) aligned GNRs in a PEO film and (c) aligned GNRs in a PEO nanofiber, both confirming the alignment as revealed by the extinction spectrum. Note: (c) has the same scale as (b).

resonance frequencies associated with the longitudinal and transverse nanorod axes. Consequently, light absorption occurs only if the incident light possesses a wavelength within the spectral band of the plasmon resonance as well as a matching polarization direction. Specifically, linearly polarized light will efficiently excite the LSRP (TSPR) only if its electric field polarization is parallel to the long (short) axis of the nanorod.[62] Such sensitivity provides a convenient means to directly observe GNR rotational motion—that is, monitoring the transmittance of a linearly-polarized, low intensity probe laser spectrally tuned to one SPR mode gives dynamic information about collective GNR orientation within the sample. This approach is particularly useful when an initial alignment of the nanorod ensemble can be created.

Fig. 1(a) displays a normalized linearly-polarized extinction spectrum of oriented GNRs embedded in the PEO composite film. The GNR-PEO sample is initially aligned parallel to the incident light polarization direction (*i.e.*, 0°), and then physically rotated in 15° increments from 0° to 90°. The reduction in the LSPR peak extinction amplitude at ~840 nm as the sample rotates from parallel to perpendicular relative alignment is due to the polarization-dependent absorption of the nanocomposite film. The TSPR is far less sensitive, but displays commensurate behavior (*i.e.*, minimum (maximum) extinction for a parallel (perpendicular) orientation). It should be noted that the polymer PEO does not possess any wavelength specific absorption in this range of the electromagnetic spectrum. Additionally, no concentration-dependent shifts in the SPR wavelengths due to interactions between GNRs are observed in the extinction spectra under the conditions employed; hence the nanorods act as plasmonically-isolated particles. Fig. 1(b) shows a transmission electron microscopy (TEM) image of the initial GNR-PEO film in which the nanorods are aligned primarily along the vertical direction (0°±8.6° from analysis of multiple images). A PEO nanofiber with embedded GNRs which are oriented along the fiber axis direction[62,63] is shown in Fig. 1(c). Hence, in both types of polymer nanocomposites, there initially exists either a local (for the nanofiber) or global (for the film) GNR orientation direction.

Experiments utilized femtosecond pulsed excitation (800 nm, <200 fs pulse width, 76 MHz repetition rate, circularly-polarized). Previous time resolved studies on similar systems indicate that for each pulse the incident optical energy is transferred to heat in the metal lattice within 100 ps.[41,64,65] Under the excitation conditions utilized here, energy is delivered to the GNRs every ~13 ns with a <200 fs duration, but the subsequent heat flow from the GNR to the polymer matrix is much slower, requiring a longer time period (*e.g.*, ~several minutes) to eventually create a steady state spatial temperature distribution from the nanoparticles outward. In the most general case, the decrease in temperature with distance from a nanoparticle heat source could include a transition between material phases of the polymer; that is, the encompassing volume of polymer immediately surrounding the particle may be heated sufficiently to undergo a melting transition (*e.g.*, for PEO, T_{melt} = 65 °C) whereas sample regions located further away could experience an increased temperature (relative to the initial ambient condition) but still remain in the solid phase. The average intensity of the pulsed source is controllably varied using neutral density filters inserted in the beam path, generating excitation at the sample over a tunable range of 5–20 mW cm^{-2}; the maximum average laser intensity used (*i.e.*, 20 mW cm^{-2}) corresponds to a peak power intensity of ~1.3 kW cm^{-2} when modeling the femtosecond pulse as a flat-top shaped impulse with a width of 200 fs.

Optical spectroscopy measurements provide direct quantitative temperature observations at various average distances from each GNR. In order to unambiguously demonstrate the resultant temperature gradient and motivate further experiments, polymer nanofibers containing GNR were subjected to excitation conditions (10 minutes of irradiation at an average intensity of 10 mW cm^{-2}), which produces a ~95 °C steady state temperature of the polymer volume immediately surrounding each GNR (*i.e.*, in the volume of GNR rotation), a larger molten region of approximately 100 nm diameter having an average temperature of 65 °C, and an average temperature in the surrounding solid polymeric region (furthest from each GNR) of 32 °C. All these regions occur within the temperature sensitive polymeric nanofiber having ~300 nm average diameter. As shown in Fig. 2, the nanofiber surface response to temperature is readily documented by gross morphological changes, where nanofibrous samples have been subjected to conventional, uniform heating on a hot plate for 10 minutes. The temperature of the polymer composite nanofibers during these experiments is confirmed by monitoring *via* the perylene internal temperature probe (discussed below), which matches the external heater (hot plate) settings. For temperatures within 15 °C of T_m (*i.e.*, >50 °C), the fibers show overt evidence of melting, whereas temperatures of 35 °C or below result in no loss of fiber morphology.

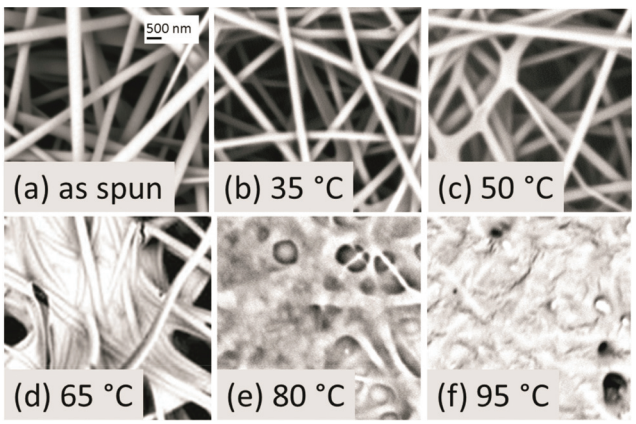

Fig. 2 SEM images of PEO nanofibrous composite mats after conventional heating for ten minutes at different temperatures show the clear destruction of the fibrous morphology that occurs under uniform spatial heating, in contrast to the preservation of the nanofiber structure under the heterogeneous temperature distribution created when using photothermal heating. For PEO, T_m = ~65 °C.

 This journal is © The Royal Society of Chemistry 2014

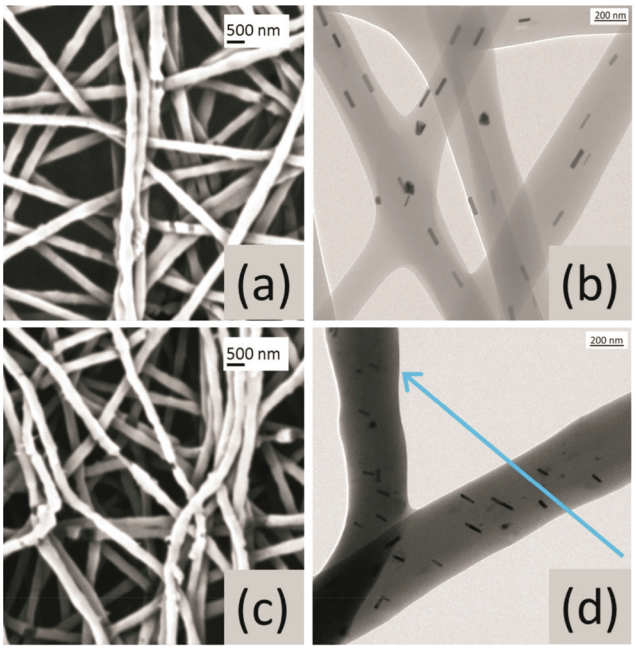

Fig. 3 (a) SEM image of randomly oriented PEO nanofibrous mat fabricated by electrospinning. (b) During fiber formation, the gold nanorods align along the fiber axis as revealed by TEM image. (c) After 10 minutes photothermal treatment by the ultrafast laser at an average intensity of 10 mW cm^{-2}, the nanofibers retain their fibrous morphology. (d) TEM images reveal photothermal treatment causes localized heating above the melting point of the polymer and the simultaneous application of an external electric field (arrow direction) enables re-orientation of the nanorods without loss of fibrous structure. Under these conditions, from rotational measurements, the average temperature at the nanorod is ~95 °C whereas far from the particle the background temperature is ~32 °C.

The initial nanofiber morphology before any thermal treatment is shown in Fig. 3 by (a) scanning electron microscopy (SEM) and (b) transmission electron microscopy (TEM), respectively. It is evident that the GNR are predominantly aligned along the nanofiber axis, as expected and discussed above. Under such aforementioned irradiation conditions, a region of molten polymer that is 100 nm in diameter would be larger than the largest dimension (length) of the GNR and consistent with observations in films (discussed below) that GNR can reorient due to this local melting of the polymer. For the ~300 nm diameter fibers utilized, creation of such a molten volume enables forced realignment of the GNR; for instance, so as to be oriented approximately perpendicular to the nanofiber axis, a configuration unachievable from direct electrospinning. Simultaneously, however, the inhomogeneous temperature distribution (in particular, the cooler solid regions further away from the particle, which remain at an average temperature of 32 °C) should allow such GNR heating and reorientation without raising the surface of the fiber above 32 °C; in other words, it would be possible to completely melt the local volume of material around the GNR while also keeping the surface (~150 nm away) at least 30 °C cooler.

Further electron microscopy images after heating the nanofibrous samples with the pulsed light source for 10 minutes at an average intensity of 10 mW cm^{-2} while an DC electric field was applied (Fig. 3(c and d)) shows that the GNRs are re-oriented in a direction approximately perpendicular to the nanofiber axis, while the fiber morphology did not change. The external electric field creates an induced dipole within the GNR; because the longitudinal polarizability of the GNR is greater than the transverse direction, the particle experiences a torque to align the nanorod long axis with the electric field direction. Without overt melting of the local polymer regions surrounding each GNR, the DC electric field has no effect on the nanorod alignment: the GNR can *only* reorient if the surrounding polymer region is at or above T_m. Conversely, however, if a large fraction of the sample volume actually was at or above T_m, obvious loss of the nanofibrous morphology would occur, such as that previously shown for hot plate heating (Fig. 2). The fact that the nanofibers remain largely intact implies that despite the complete melting of the polymer in the local volume encompassing the GNR which enables its realignment—the surface of the nanofiber *must* remain relatively cool. Furthermore, the nanofibers do not undergo curling or fusing of neighboring fibers, and porosity of the nanofibrous mat remains unchanged; all clear indications that the average temperature of the sample does not increase significantly. Thus, these observations clearly demonstrate a steady state temperature gradient must be present in the sample between regions local to the GNR and those further removed. We do note that occasional fiber breakage occurs at GNRs due to the local photothermal heating, but under most circumstances, the fibers maintain their intact cylindrical morphology as the GNRs re-orient.

2.2. Optical measurements of nanocomposite temperature

2.2.1. Perylene fluorescence amplitude ratios. We now discuss the suite of optical experiments utilized to quantify sample temperature, beginning with the techniques sensitive to the regions furthest from the particles. The use of perylene as a molecular thermometer has previously been reported.[62,66] Perylene is uniformly dispersed (0.09 wt%) throughout the nanocomposite (either fibers or films) and excited with a weak, constant intensity laser at 405 nm which spatially overlaps the femtosecond pulsed photothermal heating laser. Characteristic perylene emission spectra are presented in Fig. 4(a).

The ratio of measured emission intensity at ~462 nm (the local minimum between peaks at ~452 nm and ~479 nm referred to as the trough) to that at ~479 nm (the highest peak in the spectrum) for perylene molecules embedded in a PEO polymer matrix is a linear function of temperature. After measurement of this linear response by conventionally heating samples, the resultant calibration provides an optical means of monitoring the average sample temperature under photothermal heating. Hence, the fluorophores act as non-contact, nanoscale sensors; implementing ratiometric observations under different photothermal excitation intensities provides a

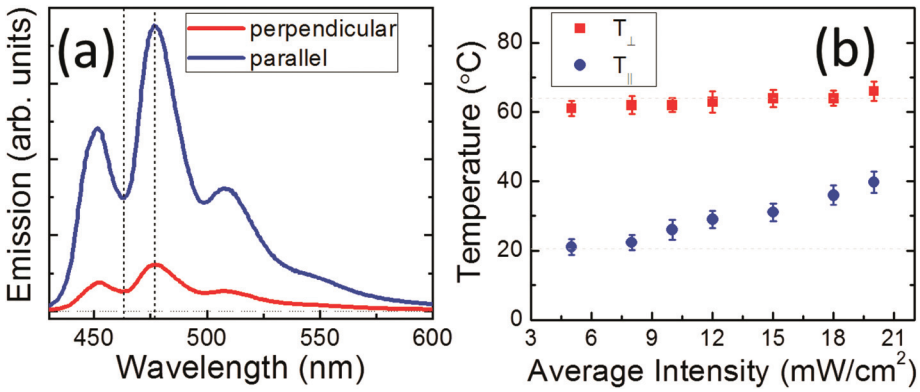

Fig. 4 Nanocomposite film samples under ultrafast pulsed excitation. (a) The characteristic perylene spectrum corresponding to parallel (blue) and perpendicular (red) emission detection for a 20 mW cm^{-2} photothermal excitation of GNRs. The differences in overall amplitude of the spectra depict the difference in populations emitting parallel or perpendicular polarized light. (b) The raw spectrum can be converted to temperature using the calibration system explained in the Experimental section, and thus corresponding to different photothermal intensities we obtain two different temperatures, $T_{\parallel}$ and $T_{\perp}$. The $T_{\parallel}$ ($T_{\perp}$) component reveals the steady-state temperature of the sample far away from (closer to) the GNRs. Dashed horizontal lines indicate room temperature and PEO T_m, respectively.

direct measurement of the average temperature value of the entire polymer film. The perylene concentration is such that perylene molecules are spaced by an average distance that is several times their longest dimension, thus they should act as a many independent non-interacting probes, as confirmed by the observed emission spectrum. However, there are many ($\sim 2 \times 10^4$) perylene molecules per GNR; volume effects dictate that most perylene molecules are located relatively far from a GNR (*i.e.*, >95% of the perylene is outside the rotation volume of the GNR). Thus the perylene measurement is particularly sensitive to the regions of the sample away from the GNR immediate vicinity. We note that no evidence of non-linear absorption by perylene under illumination by the femtosecond laser source under the conditions employed is observed and the subsequent changes to the fluorescence spectrum are completely driven by the sample temperature dynamics.

2.2.2. Polarization analysis of fluorescence. Using an approach analogous to fluorescence anisotropy measurements,[67] exciting perylene with a linearly-polarized source and resolving the polarization components of the emission gives additional information about the temperature gradient within the sample. Measurements of the perylene absorption and fluorescence spectra are consistent with well-dispersed, isolated fluorophores in the samples. A polarized continuous-wave source selectively excites the homogeneously-distributed perylene molecules from the lowest vibrational level in the S_0 electronic ground state to the first excited state S_1. Molecules with their absorptive dipole axis oriented along the polarization direction will be excited more efficiently, since those with an absorption axis oriented perpendicular to the polarization will tend not to interact with the light. After rapidly undergoing vibrational relaxation to the lowest level of the upper state and an average time delay corresponding to the excited state lifetime ($\sim$5 ns[68]), these molecules emit a Stokes-shifted photon in returning to the lower state. (For this transition in the perylene molecule, the emission dipole is almost perfectly aligned parallel to the absorptive dipole axis[69]). Several vibrational levels in the ground state are accessible, giving rise to the multi-peak spectrum displayed in Fig. 4. However, if the local polymer environment surrounding the perylene molecules is molten, this provides a rotational degree of freedom (*i.e.*, the fluorophore can physically re-orient during the excited state lifetime) which subsequently depolarizes the observed emission relative to the initial polarization direction of the excitation source. In contrast, if the perylene molecule resides in a solid region of polymer, the emission will be correlated with the original excitation polarization direction.

In the experiment, a large region of the sample is uniformly illuminated with linearly polarized light which is kept at a constant intensity for all experiments (in contrast with the ultrafast pulsed photothermal excitation which is altered to tune the temperature distribution in the sample). The resultant emission is separately measured in two orthogonal directions (parallel and perpendicular to the emission beam polarization direction). Employing the abovementioned spectral amplitude ratio analysis results in two temperatures $T_{\parallel}$ and $T_{\perp}$. Thus, the temperature reported as $T_{\perp}$ primarily reflects contributions from rotationally-active perylene molecules. In contrast, $T_{\parallel}$ will be comprised of signals predominantly from fluorophores which remained unmoving within the solid polymer matrix (*i.e.*, in environments where the molecules cannot rotate during the excited state lifetime); hence, these molecules are more likely to be located in cooler regions at larger distance from the nanorods. We note that under such dilute fluorophore loading as employed here, the molecules are well separated and short range resonant energy transfer processes (*e.g.*, FRET) are highly suppressed; moreover, no evidence of excimer emission is observed, indicating the perylene molecules are well-dispersed in the polymer matrix and few, if any aggregates, are present.

 This journal is © The Royal Society of Chemistry 2014

Fluorescence spectra for parallel and perpendicular polarized emission detection for an applied 20 mW cm^{-2} average ultrafast photothermal excitation source intensity are presented in Fig. 4(a). Each polarization direction displays the same characteristic emission spectrum – the differences in overall amplitude and shape reflects effects of temperature and relative populations (discussed below). Under different average ultrafast pulsed excitation intensities, the corresponding steady state temperature ($T_{\parallel}$ and $T_{\perp}$) from each emission polarization direction is depicted in Fig. 4(b). Values for $T_{\perp}$ have been adjusted to reflect only the region exterior to the rotation volume of the GNR, as discussed in detail below. For these excitation conditions, both $T_{\parallel}$ and $T_{\perp}$ increase steadily with exposure time of 2–10 minutes (dependent on the applied photothermal heating intensity) and then saturate at the steady state value. The $T_{\perp}$ component shows an average steady state temperature equal to or greater than T_m of the polymer matrix which is an independent, self-consistent confirmation that $T_{\perp}$ component is dominated by the contribution of perylene molecules that can rotate due to melting of the surrounding matrix. This result is also consistent with the observed capability of the GNRs to rotate under these conditions. The $T_{\parallel}$ component demonstrates that the sample volumes further from the particles experience an increase in temperature with higher average excitation intensity but remain in the solid phase for all conditions shown.

In nanocomposite films, based on the volume and known GNR concentration, the average nanorod separation is ~270 nm; thus a simple but still insightful model of the sample is to view it as a collection of spheres of polymeric material, each with a radius of 135 nm and a GNR located at the center as schematically depicted in Fig. 5. In summary, the measured $T_{\perp}$ ($T_{\parallel}$) component shown in Fig. 4 corresponds to the "inner molten region" ("outer solid region") which is schematically depicted in Fig. 5. (Note: the hottest, volume of rotation region is discussed later.) This method enables direct determination of the average temperature of the molten and solid regions of the sample and provides internal self-consistency checks of the experimental results.

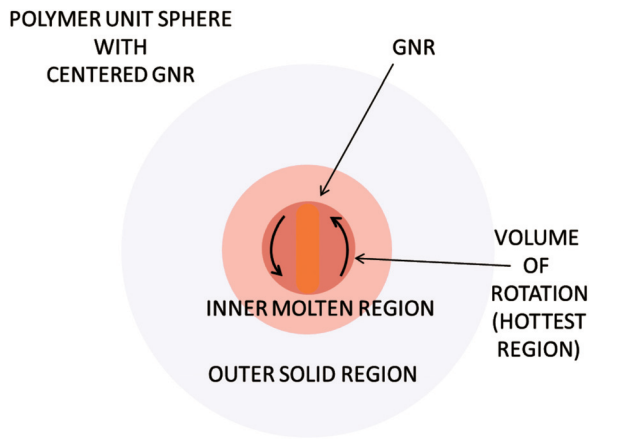

Fig. 5 Schematic depiction of the GNR's volume of rotation and the subsequent temperature zones around it based on the polarized perylene spectrum and the inter-particle distances. The volume of rotation registers the hottest temperature as recorded by the rotational spectroscopy, the inner molten region is sampled by the perpendicular perylene emission giving $T_{\perp}$, and the outer solid region corresponds to the temperature $T_{\parallel}$, as reported by parallel perylene emission.

2.2.3. Estimation of polymer melt volume. Further analysis of the amplitude of the observed fluorescence signals for the different polarizations allows an estimation of the size of the inner molten region and the ability to observe how this region expands outward for higher femtosecond pulse intensities (as a larger fraction of the sample becomes molten). In such an analysis, the absolute fluorescence intensity from the two channels is compared, taking into account the differences in perylene quantum yield with temperature (that is, molecules in the warmer regions have a greater probability of non-radiative relaxation from the excited state rather than radiative emission.) The temperature-dependent change in fluorescence quantum yield for perylene within PEO nanocomposite film samples was independently measured over the observed temperature range using a commercial spectrofluorometer, where increased non-radiative relaxation at higher temperatures reduces the quantum yield. Such measurements reveal the calibration factor which can account for the temperature-dependent loss of fluorescing efficiency. Applying such an adjustment to the integrated measured signal amplitudes corresponding to measured temperatures of the parallel (cooler regions) and perpendicular (hotter regions) polarizations more accurately describes the actual molecular populations. Subsequently, these corrected signals can then be directly related to the volume of material at the inferred temperature, under the reasonable assumption of homogeneous fluorophore dispersion within the films. Specifically, the total average volume per GNR (see Fig. 5) is known from the GNR–polymer volume fraction, thus comparing the corrected perpendicular fluorescence intensity (proportional to the volume of the molten region) to the corrected parallel intensity (proportional to the volume of solid spherical shell in Fig. 5), results in an estimate of the molten region volume.

The radius of the inner molten region as a function of the photothermal heating pulsed laser intensity is presented in Fig. 6. For this range of intensities, the inner molten region is always larger than the rotation volume of a GNR (a sphere with a radius equal to the one-half the length of the GNR, ~34 nm), which indicates that the GNR is capable of rotation under these conditions, as confirmed independently below. As the intensity increases, the size of the inner molten region grows, but molten regions from neighboring particles do not (on average) overlap, which would require a molten radius equal to one-half of the average distance between GNR (135 nm). For all photothermal intensities used here, most of the polymer sample therefore remains solid.

Based on volume calculations for the lowest (highest) intensity in Fig. 6, only 4% (10%) of the sample is molten. These molten regions are centered on the GNRs; thus enabling manipulation of the GNR (as seen in the fiber case above) without significantly affecting >90% of the sample material. In

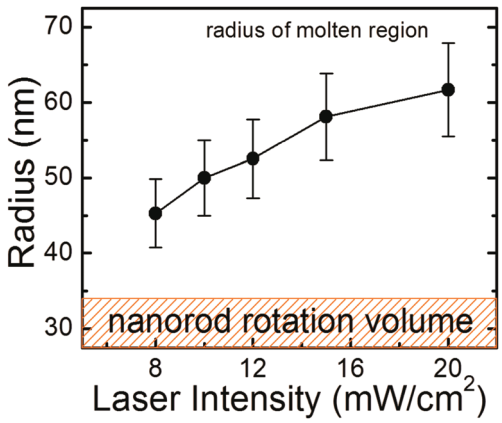

Fig. 6 The radius of the inner molten region as a function of the average pulsed laser intensity. The inner molten region is always larger than the sphere corresponding to the length of the GNR (~70 nm), and with increasing photothermal intensity the molten region increases. Although the molten volume growths with increasing intensity, it is still centered on individual GNRs without overlap from adjacent GNRs, thus enabling site-specific processing without influencing the bulk of the sample.

fact, the size of the molten region as determined *via* the perylene measurement is completely consistent with the fiber experiments summarized in Fig. 1. For an intensity of 10 mW cm^{-2}, the estimated size of the molten region is ~100 nm in diameter, centered on each GNR. This observation is fully consistent with the ability to reorient nanorods within a 300–400 nm nanofiber without melting the outer fiber surface.

2.2.4. Direct detection of ensemble GNR rotation. As a final approach to measure the temperature in the interior of the nanocomposite, the local temperature of the polymer in the immediate vicinity of the GNR can be investigated by monitoring the rotational dynamics of the nanorod within the polymer melt. This technique probes a sub-set of the inner molten region discussed above; in particular, where the polymer is intimately associated with the GNR, which can be estimated as the sub-region of polymer within the GNR rotational volume (a sphere with radius ~34 nm). Since the GNRs behave as the heat sources, it is physically reasonable that temperature of the polymer in intimate contact with the GNR is significantly warmer than the average value determined by the measurement of $T_{\perp}$, which due to volume effects is dominated by the perylene molecules at the edge (the largest radius) of the molten region. In fact for the highest (lowest) intensity shown in Fig. 6, only 14% (36%) of the perylene molecules will reside in this intimate region. Estimating the temperature of the intimate sub-region provides the ability to modify the raw $T_{\perp}$ results to reflect only the non-intimate region (resulting in the adjusted $T_{\perp}$ values in Fig. 4), which then provides three different temperature measurements in three independent regions: the intimate rotation volume, the remainder of the inner molten region, and the outer solid region. Measurement of the temperature of polymer closest to the nanorod also provides a lower limiting value for the GNR temperature.

The basic rotational temperature experiment involves (i) continuous application of the pulsed excitation that results in heating, (ii) a wait of a few minutes while the sample reaches steady state, and (iii) subsequent observation of rotation of the GNR, either due to thermally-driven rotations which result in randomization of the nanorod orientation or intentional driven realignment with an electric field applied perpendicular to the original orientation direction (thereby reorienting each GNR by 90°). Such experiments can be conducted in any circumstances where the region immediately surrounding each GNR is molten including the extreme case where the entire sample is at a uniform temperature above the melting point (*e.g.*, due to conventional heating). The rates at which the rotational diffusion occurs are representative of the viscosity and thus the temperature of the polymer melt. The approach to and achievement of steady state is determined by observing the average sample temperature in the region furthest from the heat source ($T_{\parallel}$, monitored *via* perylene thermometry) which undergoes a smooth increase and then approaches a constant, steady state final value. When $T_{\parallel}$ equilibrates, we expect that the steady state inhomogeneous temperature distribution is present throughout the sample, with different temperatures at varying distances from each GNR but with the local temperature at any given distance now constant with time; if steady state would not be achieved, then $T_{\parallel}$ would not be constant. An external homogeneous DC electric field aligned parallel to the nanorod long axes maintains the initial GNR alignment during the ultrafast laser illumination until the steady state condition is achieved, thus preventing the GNR from reorienting during the approach to the final steady state. Once the stable sample temperature (measured far from the nanorod) is achieved, the electric field direction is switched in order to facilitate GNR rotation. Since the pulsed laser is circularly-polarized, the efficiency of photothermal heating does not depend on relative GNR orientation.

The orientation of the GNR ensemble is monitored *via* a linearly-polarized amplitude modulated, low intensity probe beam (spectrally resonant with LSPR with its polarization direction oriented perpendicular to the original GNR alignment direction) passing through the GNR-PEO film sample. The transmitted light is collected on a photodiode detector whose output is fed to a lock-in amplifier referenced to the modulation frequency. Initially, the weak probe beam's transmittance through the sample is maximized, but as the nanorods reorient within the polymer melt assisted by the DC electric field, the GNRs' longitudinal axes slowly start aligning with the probe polarization direction and thereby, reduce the probe beam transmittance. Eventually, when the long axes of the GNRs are oriented parallel to the light field polarization direction, the amplitude of the transmitted probe beam is minimized (Fig. 7). Normalized transmittance $(T - T_{\min})/(T_{\max} - T_{\min})$ is plotted where $T_{\max}$ ($T_{\min}$) is determined by physically aligning the initial sample perpendicular to (along) the original alignment direction.

The transition rate from the maximum to minimum transmittance can be utilized to estimate an effective temperature

 This journal is © The Royal Society of Chemistry 2014

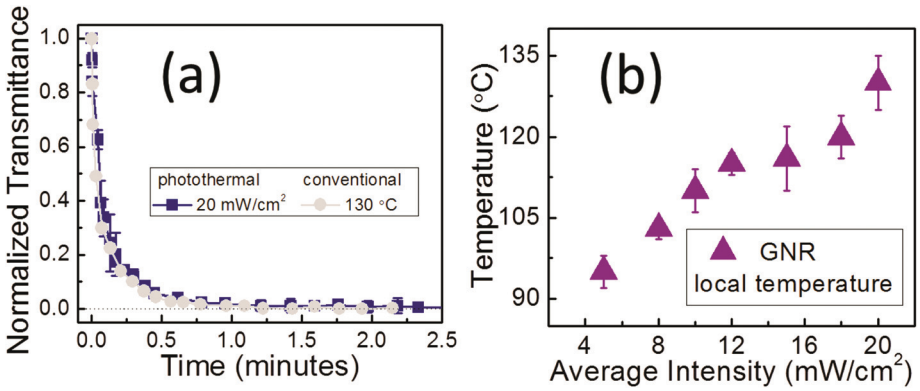

Fig. 7 (a) Normalized transmittance through the GNR–PEO nanocomposite sample when photothermally heated with 20 mW cm^{-2} and conventionally heated at 130 °C. The well-overlapped curves indicate that a good estimate of the steady state temperature of the nanocomposite at the GNRs when irradiated with 20 mW cm^{-2} is 130 °C. (b) With this approach, estimates of nanocomposite temperatures as determined by comparing rotation rates under pulsed laser intensities. GNR local temperature refers to the average temperature in the volume of rotation of the nanorod.

as follows. The polymer viscosity in the region immediately surrounding each GNR determines the rate of reorientation (the driving force is constant for all experiments). Polymer dynamics in the immediate vicinity of GNRs can vary from expected bulk polymer response.[70–73] Thus, in order to determine the temperature under photothermal heating, equivalent rotational dynamics for the nanorods can be measured when the sample is uniformly heated (*i.e.*, uniformly melted) using conventional methods, enabling a direct comparison between sample temperature and rotational rate. Fig. 7(a) shows a comparison of the measured rotational dynamics of GNRs in a nanocomposite film under ultrafast pulsed illumination having a 20 mW cm^{-2} average intensity with those displayed by nanorods in a sample conventionally heated to 130 °C. The similarity of the two curves indicates a good estimate of the temperature of the intimate sub-volume surrounding the GNRs is 130 °C under this heating condition. Hence, by matching the time-dependent observed dynamics at different laser intensities with the corresponding curves for conventionally heated samples at uniform temperatures, the temperature of the polymer in the spatial region immediately surrounding the nanorods can be estimated for the given applied photothermal excitation intensities.

Fig. 7(b) displays inferred temperatures in the intimate local vicinity of the GNRs from the measured rotation dynamics under different average illumination intensities from the ultrafast laser. As expected, the temperature in the region increases sharply with increased intensity. This temperature reflects the average temperature of the polymer melt in the volume of rotation of the nanorods. Within such small material volumes, fluctuations of temperature gradients may exist but this method integrates signals from $\sim 10^{10}$ GNRs within the probe beam volume, hence this local temperature reflects an average value of the ensemble. We note that when the sample temperature is below T_m for PEO, no change in the transmittance signal is observed and nanorod re-orientation is not possible; hence, any measured variation in transmittance unambiguously demonstrates that the GNRs are rotating and that locally in the volume of rotation (when undergoing photothermal heating), the polymer *must* be molten. This measurement can also be performed when the orthogonally-oriented DC electric field is off; when sufficiently heated the GNRs simply wander from their aligned positions, resulting in random rotation (*i.e.*, Brownian motion): such measurements yield identical inferred temperature observations when calibrated against conventionally-heated samples. Under all conditions, the rotation temperature measurement is completely model-independent and requires no assumptions about the viscosity *versus* temperature profile, or the presence or deviation from diffusive dynamics within the polymer melt. The calibration approach employed enables a direct estimation of temperature without reliance on explicit modeling of the rotational motion. As discussed below, these experimental results of temperature *versus* average distance can be compared to theoretical predictions[1] that temperature should decrease as $1/r$ with distance from the nanoparticle; this allows an independent check of the self-consistency of the different types of optical temperature measurements.

The various temperature measurements can be combined and cross-checked as follows. Modelling the nanocomposite film samples as a collection of spheres of polymeric material, each with a radius of 135 nm and a GNR located at the center (Fig. 5) within each sphere, there are three distinct regions, the spherical rotation volume (*i.e.*, the intimate sub-region of polymer in contact with the GNR), and two spherical shells: the remainder of the inner molten volume, and the outer solid region. The location of the boundary between the inner molten and outer solid region is determined from the amplitudes of the corrected fluorescence signals as shown in Fig. 4(a). The inner region is assumed spherical as the rotating nanorod could (in principle) sample polymer throughout a uniform region. If the inner molten region were very small, with a radius similar to that of the GNR, the molten region around the GNR would be elliptical; however in this case, the molten region is significantly larger than the GNR.

From the GNR rotation measurement, the average temperature of the polymer melt ($T_{rotation}$) in a concentric spherical

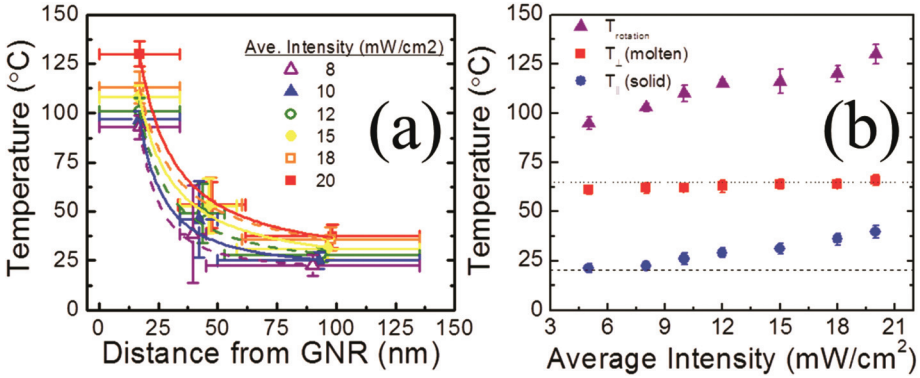

Fig. 8 (a) The distribution of temperatures associated with these three spatial regions for varying average intensities of the pulsed irradiation. (b) Summary of the results of the three measurements for temperature in the different spatial regions as the average laser intensity is increased.

volume with radius ~34 nm around the nanorod can be determined (*i.e.*, the rotation volume). The $T_{\perp}$ measurement also samples this intimate volume immediately surrounding each GNR and raw $T_{\perp}$ values (not shown) thus averages over both this small volume and the remaining larger molten region. It is thus most useful to adjust the $T_{\perp}$ value (by accounting for the volume fraction that should be reporting at T_{rotation}) so that $T_{\perp}$ only reflects the molten volume outside the rotation volume of the GNR. The resultant $T_{\perp}$ serves as a cross-check of the consistency of the different experiments. As the light intensity increases, the molten region increases in size; aside from temperature dependent differences in quantum yield, all perylene molecules in the molten region contribute equally. Thus because the volume of a spherical shell increases dramatically with radius, the temperature reported by the adjusted $T_{\perp}$ should be close to that of the temperature at the boundary between melt and solid. Indeed, the results in Fig. 8 show this effect.

When the heating laser average intensity is increased, the size of the molten regions and thus number of reporters in the molten region slowly rises, however the dominant sample temperature $T_{\parallel}$ is relatively constant, as it reflects the largest radius region, the region that remains solid but warms slightly. This is in direct contrast with the GNR rotation measurement, for instance, where the volume sampled is fixed and the temperature within this fixed volume increases with photothermal intensity. All three different average temperature measurements provide results that are self-consistent.

The distribution of temperatures associated with these three spatial regions for varying average intensities of the pulsed irradiation are presented in Fig. 8(a). Unsurprisingly, with higher excitation intensities, the temperature in each of the concentric volumes is higher. Associating each temperature with the median radius gives the temperature profile with distance as a function of pulsed irradiation intensity. The temperature profiles obtained for all the different intensities are numerically fitted and the fit parameters reveal that the temperature falls off approximately as $1/r$ where r is the distance from the center of the nanorod moving radially away from the GNR, in agreement with other experimental results and theoretical predictions.[5] Fig. 8(b) summarizes the results of the three measurements for temperature in the different spatial regions as the average laser intensity is increased.

3. Conclusion

GNRs efficiently generate heat when exposed to a femtosecond ultrafast laser tuned to a frequency corresponding to the particles' localized surface plasmon resonance. The heat generated is dissipated into the surrounding polymer environment, and depending on the incident intensity, can eventually melt local polymer regions. The average temperature of the nanorod vicinity can be inferred using the rotation of the GNRs in polymer melt. Using perylene fluorescence and implementing polarized detection for parallel and perpendicular emission, the average temperature of the bulk sample can be divided into contributions from molten and solid regions of the sample. Combining these observations provides three temperatures corresponding in a simple model to different concentric volumes of polymer around the nanorod. The resultant temperature profile suggests that the experimentally measured steady state temperature profile is consistent with the theoretically predicted decay of $1/r$ under such pulsed heating in polymers. In polymer systems with distinct morphologies, this intense heat localization can be implemented to control temperature locally without affecting the bulk morphology, as is demonstrated by intentionally re-orienting a GNR within an intact nanofiber without affecting the highly temperature-sensitive nanofiber surface. This experimental formulation provides a versatile and self-calibrated approach for mapping the temperature profile due to femtosecond photothermal heating in solid media.

4. Experimental section

4.1. Materials

Polyethylene oxide (PEO) having molecular weight of 400 kg mol^{-1} was purchased from Scientific Polymer Products.

 This journal is © The Royal Society of Chemistry 2014

Perylene (99.5%) and NaOH (98%) from Sigma Aldrich, tetraethoxysilane (99.9%) from Alfa Aesar, 2-[methoxy(polyethyleneoxy)propyl)9-12trimethoxysilane (PEG-silane) from Gelest, and methanol (UltimAR) from Macron were used for the fluorescence temperature sensors and to produce the silica coating, respectively. All chemicals were used as received without further purification. Deionized water (18.2 MΩ) was produced from a laboratory purification system (Evoqua Water Technologies). Prior to use, microscope glass coverslips (Fisherbrand, microscope cover glass 12-540B) were cleaned using a UV-ozone system (Procleaner 110, Bioforce Nanoscience).

4.2. Gold nanorod synthesis

GNRs were fabricated using a seed-mediated growth process,[55] resulting in nanoparticles with average lengths of 68 ± 7 nm, widths of 17 ± 3 nm, and ARs of 4.0 ± 0.82. The GNRs were coated with thin silica shells using a method (in preparation to be published elsewhere)[74] that give comparable results to an established method.[55,75] Surfaces of the silica-coated GNRs were PEGylated by adding PEG-silane, enabling good solubility in multiple solvents.

4.3. Nanocomposite film fabrication

PEO powder (4.0 wt%) was mixed into a GNR-methanol solution, and perylene was added (0.09 wt% in the final film) to serve as a fluorescent temperature sensor. For creation of nanocomposite film samples, this resultant solution was drop-cast onto a cleaned glass coverslip to obtain a GNR-PEO thin film with thickness of ~8 μm. For the samples discussed in this report, 2.5 wt% GNRs was used, corresponding to an average separation of 270 nm between nanorods. While drying under ambient conditions, using external electrodes a DC electric field (~20 kV cm^{-1}) is applied in order to orient the GNRs' long axes parallel to the applied field direction.

4.4. Nanocomposite fiber fabrication

Nanofibers were fabricated using traditional needle electrospinning. A PEO–GNR–perylene solution was magnetically stirred for 10 hours then electrospun using a syringe-pump (New Era Pump Systems, Model NE 500) solution-driven feed rate of 6 μL per minute with a positive needle-to-collector applied voltage of 15 kV (Glassman High Voltage, Model no. FC60R2) and a needle-to-grounded collector distance of 20 cm. The subsequent resultant nanofibers are readily collected with random fiber orientation in layers on a fixed aluminum foil, aluminum stubs, or copper grids for electron microscopy analysis, having ~250 ± 30 nm in diameter.

4.5. Sample characterization

Extinction measurements of film samples were performed using a Cary-50 absorption spectrometer. Scanning electron microscopy (SEM) images were taken using a FEI Phenom-World BV) to characterize the nanofibers. Transmission electron microscopy measurements were performed using JEOL 2000FX TEM to analyze the dimensions of the GNRs and their orientations within thin film and fiber samples. Sample fluorescence was detected using a CCD array (Sony) with a WinSpec spectrometer, with appropriately oriented polarizers to select specific relative linear polarization directions. The relative quantum efficiency of perylene doped in PEO as a function of temperature was measured using spectrofluorometer (QuantaMaster 40, Photon Technology International) with an externally controlled heated stage. The rotational temperature was calibrated using a VWR 7 × 7 CER hot plate while the rotation of the GNRs were optically monitored by the process described in the Results section.

4.6. Illumination sources

The femtosecond irradiation source was produced by a Ti:Sapphire mode-locked laser (Coherent MIRA 900F) pumped by a solid state laser (Coherent Verdi G7) at 532 nm with 7.3 W. The ultrafast pulsed light was spectrally centered at 800 ± 2 nm having a 200 fs temporal width at a 76 MHz repetition rate. The excitation beam is circularly polarized using a linear polarizer and a quarter-wave plate, then collimated and expanded to ~5 mm diameter to fully illuminate the sample. The average intensity was controllably varied using a neutral density filter, generating excitation at the sample over a facile tunable range of 5–20 mW cm^{-2}. To monitor the GNR orientation, a weak, linearly-polarized, 808 nm continuous-wave diode laser (whose polarization direction is oriented perpendicular to the original GNR alignment direction) is flywheel chopped at a 2 kHz rate. To perform temperature measurements, a 405 nm linearly-polarized continuous-wave diode laser is expanded and collimated to ~3 mm diameter to excite the homogeneously-distributed perylene molecules.

Acknowledgements

This work was supported by the National Science Foundation (grants CMMI-0829379, CMMI-106910, DMR-1056653, the Research Triangle MRSEC DMR-1121107, and the National Institutes for Health Grant 1R21HL111968-01A1,) and Sigma Xi (GIAR). The authors thank both the NC State Physics Education and Research Laboratory (EaRL) and Dr Keith Weninger for use of equipment.

References

1 A. O. Govorov and H. H. Richardson, *Nano Today*, 2007, **2**, 30–38.
2 S. Maity, L. N. Downen, J. R. Bochinski and L. I. Clarke, *Polymer*, 2011, **52**, 1674–1685.
3 T. Ming, H. J. Chen, R. B. Jiang, Q. Li and J. F. Wang, *J. Phys. Chem. Lett.*, 2012, **3**, 191–202.
4 P. K. Jain, K. S. Lee, I. H. El-Sayed and M. A. El-Sayed, *J. Phys. Chem. B*, 2006, **110**, 7238–7248.
5 G. Baffou and H. Rigneault, *Phys. Rev. B: Condens. Matter*, 2011, **84**, 035415.

6 L. Cao, D. N. Barsic, A. R. Guichard and M. L. Brongersma, *Nano Lett.*, 2007, **7**, 3523–3527.
7 P. Zijlstra, J. W. M. Chon and M. Gu, *Opt. Express*, 2007, **15**, 12151–12160.
8 G. Baffou, R. Quidant and F. Javier Garcia de Abajo, *ACS Nano*, 2010, **4**, 709–716.
9 K. C. Hribar, R. B. Metter, J. L. Ifkovits, T. Troxler and J. A. Burdick, *Small*, 2009, **5**, 1830–1834.
10 Z. W. Xiao, Q. Wu, S. D. Luo, C. Zhang, J. Baur, R. Justice and T. Liu, *Part. Part. Syst. Charact.*, 2013, **30**, 338–345.
11 H. J. Zhang, J. M. Zhang, X. Tong, D. L. Ma and Y. Zhao, *Macromol. Rapid Commun.*, 2013, **34**, 1575–1579.
12 D. A. Boyd, L. Greengard, M. Brongersma, M. Y. El-Naggar and D. G. Goodwin, *Nano Lett.*, 2006, **6**, 2592–2597.
13 H. Chen, X. Liu, H. Muthuraman, J. H. Zou, J. H. Wang, Q. Dai and Q. Huo, *Adv. Mater.*, 2006, **18**, 2876–2879.
14 A. Nitzan and L. E. Brus, *J. Chem. Phys.*, 1981, **75**, 2205–2214.
15 W. A. Challener, C. B. Peng, A. V. Itagi, D. Karns, W. Peng, Y. Y. Peng, X. M. Yang, X. B. Zhu, N. J. Gokemeijer, Y. T. Hsia, G. Ju, R. E. Rottmayer, M. A. Seigler and E. C. Gage, *Nat. Photonics*, 2009, **3**, 220–224.
16 J. W. M. Chon, C. Bullen, P. Zijlstra and M. Gu, *Adv. Funct. Mater.*, 2007, **17**, 875–880.
17 A. Stalmashonak, A. Abdolvand and G. Seifert, *Appl. Phys. Lett.*, 2011, **99**, 201904.
18 M. A. Ullah, X. P. Li, X. M. Cheng, X. J. Hao, Y. H. Su, J. S. Ma and M. Gu, *Opt. Express*, 2012, **20**, 24516–24523.
19 P. Zijlstra, J. W. M. Chon and M. Gu, *Nature*, 2009, **459**, 410–413.
20 D. Pissuwan, S. M. Valenzuela and M. B. Cortie, *Trends Biotechnol.*, 2006, **24**, 62–67.
21 S. Lal, S. E. Clare and N. J. Halas, *Acc. Chem. Res.*, 2008, **41**, 1842–1851.
22 P. K. Jain, I. H. El-Sayed and M. A. El-Sayed, *Nano Today*, 2007, **2**, 18–29.
23 P. K. Jain, X. H. Huang, I. H. El-Sayed and M. A. El-Sayed, *Acc. Chem. Res.*, 2008, **41**, 1578–1586.
24 N. G. Khlebtsov and L. A. Dykman, *J. Quant. Spectrosc. Radiat. Transfer*, 2010, **111**, 1–35.
25 M. Delcea, N. Sternberg, A. M. Yashchenok, R. Georgieva, H. Baumler, H. Mohwald and A. G. Skirtach, *ACS Nano*, 2012, **6**, 4169–4180.
26 A. M. Alkilany, L. B. Thompson, S. P. Boulos, P. N. Sisco and C. J. Murphy, *Adv. Drug Delivery Rev.*, 2012, **64**, 190–199.
27 T. L. Doane and C. Burda, *Chem. Soc. Rev.*, 2012, **41**, 2885–2911.
28 N. Harris, M. J. Ford, P. Mulvaney and M. B. Cortie, *Gold Bulletin*, 2008, **41**, 5–14.
29 H. J. Chen, L. Shao, Q. Li and J. F. Wang, *Chem. Soc. Rev.*, 2013, **42**, 2679–2724.
30 M.-F. Tsai, S.-H. G. Chang, F.-Y. Cheng, V. Shanmugam, Y.-S. Cheng, C.-H. Su and C.-S. Yeh, *ACS Nano*, 2013, **7**, 5330–5342.
31 A. N. Volkov, C. Sevilla and L. V. Zhigilei, *Appl. Surf. Sci.*, 2007, **253**, 6394–6399.
32 J. Baumgart, L. Humbert, E. Boulais, R. Lachaine, J. J. Lebrun and M. Meunier, *Biomaterials*, 2012, **33**, 2345–2350.
33 E. Boulais, R. Lachaine, A. Hatef and M. Meunier, *J. Photochem. Photobiol., C*, 2013, **17**, 26–49.
34 E. Y. Lukianova-Hleb, A. Belyanin, S. Kashinath, X. W. Wu and D. O. Lapotko, *Biomaterials*, 2012, **33**, 1821–1826.
35 E. Y. Lukianova-Hleb, A. P. Samaniego, J. G. Wen, L. S. Metelitsa, C. C. Chang and D. O. Lapotko, *J. Controlled Release*, 2011, **152**, 286–293.
36 M. Schomaker, J. Baumgart, A. Ngezahayo, J. r. Bullerdiek, I. Nolte, H. Murua Escobar, H. Lubatschowski and A. Heisterkamp, *Plasmonic perforation of living cells using ultrashort laser pulses and gold nanoparticles*, 2009.
37 E. Boulais, R. Lachaine and M. Meunier, *J. Phys. Chem. C*, 2013, **117**, 9386–9396.
38 R. Lachaine, E. Boulais, E. Bourbeau and M. Meunier, *Appl. Phys. A: Mater. Sci. Process.*, 2013, **112**, 119–122.
39 E. Boulais, R. Lachaine and M. Meunier, *Nano Lett.*, 2012, **12**, 4763–4769.
40 S. Link, C. Burda, B. Nikoobakht and M. A. El-Sayed, *J. Phys. Chem. B*, 2000, **104**, 6152–6163.
41 O. Ekici, R. K. Harrison, N. J. Durr, D. S. Eversole, M. Lee and A. Ben-Yakar, *J. Phys. D: Appl. Phys.*, 2008, **41**, 11.
42 S. Hashimoto, D. Werner and T. Uwada, *J. Photochem. Photobiol., C*, 2012, **13**, 28–54.
43 G. Baffou, P. Berto, E. B. Urena, R. Quidant, S. Monneret, J. Polleux and H. Rigneault, *ACS Nano*, 2013, **7**, 6478–6488.
44 M. I. Tribelsky, A. E. Miroshnichenko, Y. S. Kivshar, B. S. Luk'yanchuk and A. R. Khokhlov, *Phys. Rev. X*, 2011, **1**, 021024.
45 B. S. Luk'yanchuk, A. E. Miroshnichenko, M. I. Tribelsky, Y. S. Kivshar and A. R. Khokhlov, *New J. Phys.*, 2012, **14**, 093022.
46 A. Pyatenko, H. Q. Wang, N. Koshizaki and T. Tsuji, *Laser Photonics Rev.*, 2013, **7**, 596–604.
47 N. Zeng and A. B. Murphy, *Nanotechnology*, 2009, **20**, 375702.
48 G. Bisker and D. Yelin, *J. Opt. Soc. Am. B*, 2012, **29**, 1383–1393.
49 L. Rahimi, A. R. Bahrampour and G. P. Pepe, *J. Phys. D: Appl. Phys.*, 2012, **45**, 475306.
50 M. Rashidi-Huyeh and B. Palpant, *J. Appl. Phys.*, 2004, **96**, 4475–4482.
51 P. Keblinski, D. G. Cahill, A. Bodapati, C. R. Sullivan and T. A. Taton, *J. Appl. Phys.*, 2006, **100**, 054305.
52 V. Kotaidis, C. Dahmen, G. von Plessen, F. Springer and A. Plech, *J. Chem. Phys.*, 2006, **124**, 184702–184707.
53 V. V. Ramanan, K. C. Hribar, J. S. Katz and J. A. Burdick, *Nanotechnology*, 2011, **22**, 9.
54 Y. Son, J. Yeo, H. Moon, T. W. Lim, S. Hong, K. H. Nam, S. Yoo, C. P. Grigoropoulos, D. Y. Yang and S. H. Ko, *Adv. Mater.*, 2011, **23**, 3176–3181.

This journal is © The Royal Society of Chemistry 2014

55 K. A. Kozek, K. M. Kozek, W. C. Wu, S. R. Mishra and J. B. Tracy, *Chem. Mater.*, 2013, **25**, 4537–4544.

56 C. F. Bohren and D. R. Huffman, *Absorption and scattering of light by small particles*, John Wiley & Sons, Inc., New York, 1998.

57 P. Zijlstra, M. van Stee, N. Verhart, Z. Gu and M. Orrit, *Phys. Chem. Chem. Phys.*, 2012, **14**, 4584–4588.

58 C. L. Murphy and C. J. Orendorff, *Adv. Mater.*, 2005, **17**, 2173–2177.

59 J. Perez-Juste, B. Rodriguez-Gonzalez, P. Mulvaney and L. M. Liz-Marzan, *Adv. Funct. Mater.*, 2005, **15**, 1065–1071.

60 X. F. Lu, C. Wang and Y. Wei, *Small*, 2009, **5**, 2349–2370.

61 C. J. Luo, S. D. Stoyanov, E. Stride, E. Pelan and M. Edirisinghe, *Chem. Soc. Rev.*, 2012, **41**, 4708–4735.

62 S. Maity, K. A. Kozek, W. C. Wu, J. B. Tracy, J. R. Bochinski and L. I. Clarke, *Part. Part. Syst. Charact.*, 2013, **30**, 193–202.

63 K. E. Roskov, K. A. Kozek, W. C. Wu, R. K. Chhetri, A. L. Oldenburg, R. J. Spontak and J. B. Tracy, *Langmuir*, 2011, **27**, 13965–13969.

64 W. Huang and M. A. El-Sayed, *Eur. Phys. J.: Spec. Top.*, 2008, **153**, 223–230.

65 S. Link and M. A. El-Sayed, *J. Phys. Chem. B*, 1999, **103**, 8410–8426.

66 S. Maity, J. R. Bochinski and L. I. Clarke, *Adv. Funct. Mater.*, 2012, **22**, 5259–5270.

67 J. R. Lakowicz, *Principles of Fluorescence Spectroscopy*, Springer, New York, 2006.

68 R. L. Christensen, R. C. Drake and D. Phillips, *J. Phys. Chem.*, 1986, **90**, 5960–5967.

69 D. W. Piston, T. Bilash and E. Gratton, *J. Phys. Chem.*, 1989, **93**, 3963–3967.

70 J. Choi, M. J. A. Hore, J. S. Meth, N. Clarke, K. I. Winey and R. J. Composto, *ACS Macro Lett.*, 2013, **2**, 485–490.

71 C. C. Lin, S. Gam, J. S. Meth, N. Clarke, K. I. Winey and R. J. Composto, *Macromolecules*, 2013, **46**, 4502–4509.

72 J. T. Kalathi, U. Yamamoto, K. S. Schweizer, G. S. Grest and S. K. Kumar, *Phys. Rev. Lett.*, 2014, **112**, 108301.

73 U. Yamamoto and K. S. Schweizer, *J. Chem. Phys.*, 2011, **135**, 16.

74 W.-C. Wu and J. B. Tracy, unpublished work.

75 I. Gorelikov and N. Matsuura, *Nano Lett.*, 2008, **8**, 369–373.

This journal is © The Royal Society of Chemistry 2014